Binary neutron star mergers in fully general relativistic simulations

Masaru Shibata* and Kōji Uryū†

*Graduate School of Arts and Sciences, University of Tokyo, Komaba, Meguro 153-8902, Japan

†Department of Physics, University of Wisconsin-Milwaukee, P.O. Box 413, Milwaukee, WI53201, USA

Abstract. We perform 3D numerical simulations for merger of equal mass binary neutron stars in full general relativity preparing irrotational binary neutron stars in a quasiequilibrium state as initial conditions. Simulations have been carried out for a wide range of stiffness of equations of state and compactness of neutron stars, paying particular attention to the final products and gravitational waves. We take a fixed uniform grid in Cartesian coordinates with typical grid size $(293, 293, 147)$ in (x, y, z) assuming a plane symmetry with respect to the equatorial plane. A result of one new large-scale simulation performed with grid size $(505, 505, 253)$ is also presented.

We find that the final product depends sensitively on the initial compactness of the neutron stars: In a merger between sufficiently compact neutron stars, a black hole is formed in a dynamical timescale. As the compactness is decreased, the formation timescale becomes longer and longer. For less compact cases, a differentially rotating massive neutron star is formed instead of a black hole. In the case of black hole formation, the disk mass around the black hole appears to be smaller than 1% of the total rest mass. It is also indicated that waveforms of high-frequency gravitational waves after merger depend strongly on the compactness of neutron stars.

I INTRODUCTION

Interest in the merger phase of binary neutron stars has been stimulated by the prospect of future observation of extragalactic, close binary neutron stars by gravitational wave detectors [1]. A statistical study indicates that mergers of binary neutron stars may occur at a few events per year within a distance of a few hundred Mpc [2]. Since the amplitude of gravitational waves from a binary of mass $\sim 3M_\odot$ (where $M_\odot$ denotes the solar mass) at a distance of $\sim$ 100Mpc can be $\sim 10^{-22} - 10^{-21}$, the merger of binaries is a promising source for gravitational wave detectors. Although the frequency of gravitational waves in the merging regime will be larger than 1kHz (see Sec. IV) and hence lies beyond the upper end of an accessible frequency range of laser interferometers such as LIGO for a typical event at a distance $\sim$ 100Mpc, it may be observed using specially designed narrow band interferometers or resonant-mass detectors [1]. Future observations, although they may not be done in

near future, will provide valuable information about merger mechanisms and final products of binary neutron stars.

Interest has also been stimulated by a hypothesis about the central engine of γ-ray bursts (GRBs) [3]. Recently, some of GRBs have been found to be of cosmological origin [4]. In cosmological GRBs, the central sources must supply a large amount of the energy $\geq 10^{50}$ ergs in a very short timescale of order from a millisecond to a second. It has been suggested that the merger of binary neutron stars is a likely candidate for the powerful central source [3]. In the typical hypothetical scenario, the final product should be a system composed of a rotating black hole surrounded by a massive disk of mass $> 0.1 M_{\odot}$, which could supply a large amount of energy by neutrino processes or by extracting the rotational energy of the black hole [3].

To investigate merger of binary neutron stars theoretically, numerical simulation appears to be unique promising approach. Considerable effort has been made for this in the framework of Newtonian and post-Newtonian approximation (see, e.g., [5]). Although these simulations have clarified a wide variety of physical features which are important during the merger of binary neutron stars, a fully general relativistic (GR) treatment is obviously necessary for determining the final product and associated gravitational waves because GR effects are crucial.

Effort has been made for constructing a reliable code for 3D hydrodynamic simulation in full general relativity (see, e.g., [6–8]). Recently, the authors have succeeded in constructing a numerical code in which stable and fairly accurate simulations are feasible [8]. Applying the newly developed code, the authors and collaborators have been performing fully GR simulations for a wide variety of astrophysical problems [8–12]. In this paper, we present some of our recent results with regard to the merger of binary neutron stars.

The paper is organized as follows. In Sec. II, we summarize our formulation in 3D numerical relativity. In Sec. III, we briefly describe how to give initial conditions. In Sec. IV, numerical results with regard to merger of binary neutron stars are presented, paying particular attention to the final product and gravitational waveforms. Sec. V is devoted to a summary. Throughout this paper, we adopt the units $G = c = 1$ where G and c denote the gravitational constant and speed of light, respectively. We use Cartesian coordinates $x^k = (x, y, z)$ as the spatial coordinates; t denotes coordinate time. In the following, BH and NS denote black hole and neutron star, respectively.

II SUMMARY OF THE FORMULATION

We perform hydrodynamic simulations in full general relativity using (3+1) formalism. We use the same formulation and gauge conditions as in our previous works [8,13], to which the reader may refer for details and basic equations. The fundamental variables used in this paper are ρ: rest mass density, ε: spe-

cific internal energy, P: pressure, u^μ: four velocity, $v^k = u^k/u^t$, $\Omega = v^\varphi$, α: lapse function, β^k: shift vector, γ_{ij}: three metric, $\gamma = e^{12\phi} = \det(\gamma_{ij})$, $\tilde{\gamma}_{ij} = e^{-4\phi}\gamma_{ij}$, K_{ij}: extrinsic curvature. Definitions of several quantities are also found in Table 1.

Geometric variables, ϕ, $\tilde{\gamma}_{ij}$, the trace of the extrinsic curvature $K_k{}^k \equiv K_{ij}\gamma^{ij}$, a tracefree part of the extrinsic curvature $\tilde{A}_{ij} \equiv e^{-4\phi}(K_{ij} - \gamma_{ij}K_k{}^k/3)$, as well as three auxiliary functions $F_i \equiv \partial_j\tilde{\gamma}_{ij}$, where ∂_j is the partial derivative, are evolved with an unconstrained evolution code in a modified form of the ADM formalism [14]. GR hydrodynamic equations are evolved using a van Leer scheme for the advection terms [15] adding artificial viscous terms [8]. Violations of the Hamiltonian constraint and conservation of mass and angular momentum are monitored to check numerical accuracy. Reliability of the code has been checked by several test calculations, including spherical collapse of dust, stability of spherical neutron stars, and the stable evolutions of rigidly and rapidly rotating neutron stars which have been described in [8].

We adopt a Γ-law equation of state $P = (\Gamma - 1)\rho\varepsilon$ where Γ is the adiabatic constant. For isentropic configurations the equation of state can be rewritten in the polytropic form $P = \kappa\rho^\Gamma$ and $\Gamma = 1 + 1/n$ where κ is the polytropic constant and n the polytropic index. This is the form that we use for constructing quasiequilibrium states as initial conditions. We adopt $n = 2/3$, $4/5$, 1, and $5/4$ as a reasonable qualitative approximation to a moderately stiff, nuclear equation of state.

Instead of ρ and ε we numerically evolve the densities $\rho_* \equiv \rho\alpha u^0 e^{6\phi}$ and $e_* \equiv (\rho\varepsilon)^{1/\Gamma}\alpha u^0 e^{6\phi}$ as the hydrodynamic variables [8]. In our numerical method, the total rest mass of the system

$$M_* = \int d^3x \rho_*. \tag{1}$$

is automatically conserved.

The time slicing and spatial gauge conditions we use in this paper for the lapse and shift are the same as those adopted in our series of papers [8–13]; i.e. we impose an "approximate" maximal slice condition ($K_k{}^k \simeq 0$) and an "approximate" minimum distortion gauge condition ($\tilde{D}_i(\partial_t\tilde{\gamma}^{ij}) \simeq 0$ where $\tilde{D}_i$ is the covariant derivative with respect to $\tilde{\gamma}_{ij}$; see [13]).

III INITIAL CONDITION

Even just before merger, binary neutron stars are considered to be in a quasiequilibrium state because the timescale of gravitational radiation reaction $\sim 5/\{64\Omega(M_g\Omega)^{5/3}\}$ [16], where M_g and Ω denote the total mass of the system and the orbital angular velocity of the binary neutron stars, is several times longer than the orbital period (cf. Table 1). Thus, for a realistic simulation of the merger, we should prepare a quasiequilibrium state as the initial condition.

Model	C	$\bar{\rho}_{\rm max}$	M_*	M_g	q	X	R_τ	$C_{\rm mass}$	L/M_g	Products
(A)	0.12	0.139	0.186	0.173	1.03	0.090	5.1	0.58	37.5	NS
(B)	0.14	0.169	0.216	0.198	0.98	0.106	3.4	0.67	31.1	marginal
(C)	0.16	0.202	0.244	0.220	0.93	0.124	2.3	0.75	26.3	BH

TABLE 1. A list of quantities for initial conditions of irrotational binary neutron stars with $\Gamma = 2.25$. The compactness of each star in isolation $C \equiv (M/R)_\infty$, the maximum density $\bar{\rho}_{\rm max} \equiv \kappa^n \rho_{\rm max}$, total rest mass $\bar{M}_* \equiv \kappa^{-n/2} M_*$, gravitational mass at $t = 0$ $\bar{M}_g \equiv \kappa^{-n/2} M_g$, $q \equiv J/M_g^2$ where J is the total angular momentum, compactness of orbit $X \equiv (M_g\Omega)^{2/3} (\sim M_g/a$ where a is orbital separation), approximate ratio of the emission timescale of gravitational waves to the orbital period $R_\tau \equiv 5(M_g\Omega)^{-5/3}/128\pi$, ratio of the rest mass of each star to the maximum allowed mass for a spherical star $C_{\rm mass} \equiv M_*/2M_{*\,\rm max}^{\rm sph}$, location of outer boundaries L along three axes in units of M_g (i.e., L/M_g) for simulations with $(293, 293, 147)$ grid size, and final products are shown. All quantities are normalized by κ to be non-dimensional: We can rescale by appropriately choosing κ. Here, $M_{*\,\rm max}^{\rm sph}$ denotes the maximum allowed mass of a spherical star ($\kappa^{-n/2} M_{*\,\rm max}^{\rm sph} \simeq 0.162$ at $\bar{\rho}_{\rm max} \simeq 0.52$).

Since the viscous timescale in the neutron star is much longer than the evolution timescale associated with gravitational radiation, the vorticity of the system conserves in the late inspiraling phase of binary neutron stars [17]. Furthermore, the orbital period just before the merger is about 2msec which is much shorter than the spin period of typical neutron stars, implying that even if the spin of neutron star would exist at a distant orbit and conserve throughout the subsequent evolution, it could be negligible at the merger phase in most cases. Thus, it is quite reasonable to assume that the velocity field of neutron stars just before the merger is irrotational.

To prepare quasiequilibrium states, we assume the existence of a helicoidal Killing vector in the form, $\ell^\mu = (1, -y\Omega, x\Omega, 0)$. For irrotational fluid, the hydrostatic equation is integrated to give a Bernoulli type equation in the presence of ℓ^μ [18], resulting in a great simplification for handling the hydrodynamic equations.

Currently, we restrict our attention to initial conditions satisfying $\tilde{\gamma}_{ij} = \delta_{ij}$, $\partial_t \tilde{\gamma}_{ij} = 0$ and $K_k{}^k = 0$. The initial conditions for geometric variables are obtained by solving the Hamiltonian and momentum constraint equations, and equations for gauge conditions. In this case, the basic equations reduce to two scalar elliptic type equations for α and $\psi (= e^\phi)$ and one vector elliptic type equation for β^k [19].

The coupled equations of Bernoulli type equation and elliptic type equations for metric are solved using the method developed by Uryū and Eriguchi [19]. Several test results and scientific results are found in [19] and [20].

IV RESULTS

We have performed simulations for $\Gamma = 1.8$, 2.0, 2.25 and 2.5. The results for $\Gamma = 2$ have been already presented in [11]. In this manuscript, we show results for $\Gamma = 2.25$ which have recently obtained. In Table 1, we list several quantities which characterize the quasiequilibrium state of irrotational binary neutron stars used as initial conditions. All the quantities are scaled with respect to κ (in units of $c = G = 1$) to be non-dimensional. We choose binaries at the innermost orbits for which the Lagrange points appear at the inner edge of neutron stars [20]. To induce merger, we reduce the angular momentum J by $\sim 2 - 3\%$ (see discussion below). The gravitational mass M_g and non-dimensional angular momentum parameter $q \equiv J/M_g^2$ listed in Table 1 are calculated from initial data sets which are recomputed by solving constraint equations after the reducing of J.

We have performed simulations using a fixed uniform grid assuming reflection symmetry with respect to the equatorial plane. The simulations were mainly performed using FACOM VPP300/16R. In this case, the typical grid size was $(293, 293, 147)$ in (x, y, z). One large-scale simulation was recently performed using FACOM VPP5000 with $(505, 505, 253)$ grid size to enlarge the computational region. In both cases, the grid spacing is identical and determined from the condition that major diameter of each star is covered with ~ 33 grid points initially. The computational time for one simulation was typically ~ 100CPU hours for $\sim 10^4$ timesteps. Test simulations were performed with $(193, 193, 97)$ grid size on FACOM VX/4R to check the convergence of numerical results.

The wavelength of gravitational waves at $t = 0$ is computed as

$$\lambda_{t=0} \equiv \frac{\pi}{\Omega} \simeq 100 M_g \left(\frac{X}{0.1}\right)^{-3/2}, \tag{2}$$

where $X \equiv (M_g\Omega)^{2/3}$ denotes a compactness of orbits (cf. Table 1). To accurately extract the waveform near outer boundaries, $\lambda_{t=0}$ should be shorter than the size of the computational region along three axes L. However, as found in Table 1, this condition is not satisfied since taking such a large computational region is a very difficult task in the present restricted computational resources: $\lambda_{t=0}$ is typically $\sim L/3$ with $(293, 293, 147)$ grid size. Even with $(505, 505, 253)$ grid size, $\lambda_{t=0}$ is $\sim 2L/3$. This implies that gravitational waves in the early phase cannot be accurately computed. However, the wavelength of quasi-periodic waves of the merged object excited during merger (see Fig. 6) is much shorter than the wavelength of binaries in quasiequilibrium and L. Therefore, the waveforms in the late phase to which we here pay main attention can be computed fairly accurately.

As found in [20], orbits of all irrotational binaries with $\Gamma \lesssim 2.25$ are stable and the merger in reality should be triggered by radiation reaction of

gravitational waves. To take into account the gravitational radiation reaction approximately, we use the following method. Using the quadrupole formula, we can estimate the angular momentum loss in one orbital period $\Delta J(> 0)$ as $4\pi M_g X^2/5$ [16] and hence can write the ratio of ΔJ to the total angular momentum as

$$\frac{\Delta J}{J} = \frac{4\pi}{5q} X^2 = 0.025 \left(\frac{1}{q}\right)\left(\frac{X}{0.1}\right)^2. \tag{3}$$

Thus, we initially reduce the angular momentum by $\sim 2 - 3\%$.

In Figs. 1 and 2, we display the density contour lines and velocity vectors for ρ_* and v^i at selected timesteps for simulations of models (A) and (C). For (A) the final product is a massive neutron star. For (C) a black hole is formed and the apparent horizon is able to be located (thick solid circle in the last panel).

The total rest mass of the binary for model (A) is $\sim 20\%$ larger than the maximum allowed value of a spherical star in isolation. Even with such large mass, the merged object does not collapse to a black hole. As indicated in Fig. 1, the merger proceeds very mildly, because the approaching velocity at the contact of two stars is not very large. Consequently, the shock heating is not very important in merging. This implies that the rotational centrifugal force plays an important role for supporting the self-gravity of such supramassive outcome. To illustrate the importance of the rotation for the supramassive neutron star, the angular velocity along x and y axes and density contour lines in x-z slices are displayed in Fig. 3. It is found that the supramassive neutron star is differentially rotating and consequently has a highly flattened configuration. Fig. 3(a) shows that the magnitude of the angular velocity in the inner region is of order of the Kepler velocity, i.e., $\Omega M_g = O[(M_g/R)^{3/2}]$ where R denotes the typical radius of the merged object.

All these results are qualitatively the same as those found in simulations for $\Gamma = 2$ [11]. However, the results are quantitatively different. For $\Gamma = 2$, the maximum allowed rest mass for formation of a massive neutron star after merger is $\sim 1.5 M^{\rm sph}_{*\rm max}$ where $M^{\rm sph}_{*\rm max}$ denotes the maximum allowed rest mass of a spherical star in isolation for a fixed value of Γ. As shown here, the threshold is slightly smaller as $\sim 1.3 - 1.4 M^{\rm sph}_{*\rm max}$ for $\Gamma = 2.25$ (we determine that model (B) is located near the threshold; see below), and we have found that it is $\sim 1.6 - 1.7 M^{\rm sph}_{*\rm max}$ for $\Gamma = 1.8$. Thus, the threshold value depends on the stiffness of the equation of state.

It should be noted that the supramassive neutron star formed is temporarily stable, but not forever. It will eventually collapse to a black hole as argued in [10].

For models (B) and (C) in which $C \geq 0.14$, a black hole is formed. However, the formation process is slightly different between models (B) and (C). For model (C), a black hole is quickly formed after the first contact of two stars. On the other hand, for model (B), the merged object quasi-radially oscillates

for a couple of times after the first contact instead of prompt formation of black hole. Indeed, as shown in Fig. 4, the lapse function at $r = 0$ does not quickly approach to zero in this case. The collapse toward a black hole seems to occur after dissipating the angular momentum by gravitational radiation. The difference with regard to the formation process of black holes is reflected in gravitational waveforms (cf. Fig. 6).

In Fig. 4, we also show time evolution of α at $r = 0$ for simulations with (193,193,96) grid size. It is found that the results do not contradict with those with (293,293,147) grid size, and convergence is achieved fairly well. However, with lower resolution, the numerical dissipation of the angular momentum is larger so that the merger happens earlier than that for higher resolution. Also, high density peaks are captured less accurately because of larger numerical diffusion. For even lower resolution, the merger for model (B) could avoid immediate collapse and form a massive neutron star because of large diffusion. Thus, we deduce that the total rest mass of model (B) is near a threshold for formation of black hole. To determine the threshold of the total rest mass for black hole formation more accurately, better-resolved numerical simulations are necessary.

In the outcome of model (C), the rest mass outside the apparent horizon is less than 1% of the total. This implies that the rest mass of the disk around the black hole is very small. For model (B), we were not able to determine the apparent horizon before the computation crashed. However, we found that the mass fraction outside spheres of a fixed coordinate radius (e.g., $r = 1.5$ and $3M_g$) is decreasing with time to be very small. Thus, we expect that the mass of the disk is also very small in this case. In the following, we describe the reason for these results.

In Fig. 5, we show the mass spectrum with respect to the specific angular momentum $M_*(j)/M_*$ at $t = 0$ [20] for models (B) and (C). Here, j is the specific angular momentum $(1 + \varepsilon + P/\rho)u_\varphi$ and $M_*(j)$ is defined as

$$M_*(j) = \int_{j'>j} d^3x' \rho_*(x') \quad \text{and} \quad M_*(0) = M_*. \tag{4}$$

It is found that there is no fluid element for which $j/M_g > 1.6$.

As we found in the simulations, quite a large fraction of the fluid elements are swallowed in the black hole. Gravitational radiation carries the energy from the system in particular in the early phase, but it should be less than 1% of M_g according to the quadrupole formula (see, e.g., [13]). Thus, the mass of the black holes is approximately equal to the initial value. On the other hand, the angular momentum may be dissipated by gravitational waves by about 10% of the initial value. These facts imply that $q = J/M_g^2$ should slightly decrease from the initial value to be $q \sim 0.9$ for both models. The specific angular momentum of a test particle in the innermost stable circular orbit around a Kerr black hole of mass M_g and $q = 0.9$ (0.95) is $\simeq 2.1M_g$ ($1.9M_g$). Therefore, *any fluid element of irrotational binary neutron stars just before*

the merger does not have large specific angular momentum enough to form a disk around the formed black hole. For the disk formation, certain transport mechanism of the angular momentum such as hydrodynamic interaction is necessary. Since the black holes are formed in the dynamical timescale of the system, the mechanism has to be very effective to transport the angular momentum by more than 30% in such short timescale. However, such rapid process is unlikely to happen as indicated in the present simulations.

To observe gravitational waveforms, we extract + and × gravitational waves along z-axis defined as

$$\bar{h}_+ \equiv \frac{\tilde{\gamma}_{xx} - \tilde{\gamma}_{yy}}{2}\left(\frac{r}{M_g}\right)\left(\frac{M}{R}\right)^{-1}_{\infty}, \text{ and } \bar{h}_\times \equiv \tilde{\gamma}_{xy}\left(\frac{r}{M_g}\right)\left(\frac{M}{R}\right)^{-1}_{\infty}. \tag{5}$$

In Fig. 6 (a), we show $\bar{h}_\times$ as a function of retarded time near the outer boundary for models (A)–(C) with $(293, 293, 147)$ grid size. To illustrate the effect of the location of outer boundaries, we show $\bar{h}_+$ and $\bar{h}_\times$ for simulations with $(505, 505, 253)$ and (293,293,147) grid sizes for model (C) in Fig. 6(b). Note again that outer boundaries along each axis reside inside the wave zone in the early stage of the simulation. This effect results in the underestimation of the wave amplitude for $t - z_{\rm obs} \lesssim P_{t=0}$ where $P_{t=0}$ is the orbital period at $t = 0$ as shown in Fig. 6(b) (compare results in two different grid sizes). According to a second post Newtonian study [21], the maximum wave amplitude of $\bar{h}_{+,\times}$ at $t \sim 0$ should be ~ 0.7. Thus, with (293, 293, 147) grid size, the wave amplitude is underestimated by a factor of 2. However, with larger grid size in which $L/\lambda_{t=0} \sim 2/3$, the factor of the underestimation is $\sim 10\%$, indicating that fairly accurate waveform could be calculated with slightly larger grid size with $L/\lambda_{t=0} \sim 1$.

For $t - z_{\rm obs} \gtrsim P_{t=0}$, on the other hand, L is smaller than gravitational wavelength because the characteristic wavelength becomes short after the merger starts. Therefore, the waveforms in the late phase are considered to be fairly accurate. Indeed, the wave amplitudes for two simulations of different grid sizes agree well.

In the case of massive neutron star formation, quasi-periodic gravitational waves of a fairly large amplitude, which are excited due to the non-axisymmetric oscillations of the merged object, are emitted after the merger. Since the radiation reaction timescale is much longer than the dynamical (rotational) timescale of the system, the quasi-periodic waves will be emitted for many rotational cycles.

Even for the case of black hole formation, quasi-periodic gravitational waves are excited due to the non-axisymmetric oscillation of merged objects before collapse to a black hole. Since the computation crashed soon after the formation of the apparent horizon, we cannot draw definite conclusion with regard to gravitational waves in the last phase. However, we can expect that after the formation of a black hole, its quasi-normal modes are excited and gravitational

waves will damp eventually. Since the formation timescale of the black hole is different between models (B) and (C) depending on initial compactness of neutron stars, duration of the quasi-periodic waves induced by non-axisymmetric oscillations of the transient merged objects is also different. The wavelength of the quasi-periodic oscillation is ~ 3 times shorter than $\lambda_{t=0}$, and thus, the typical frequency can be estimated as

$$f \simeq 2.0\mathrm{kHz}\left(\frac{2.8M_\odot}{M_g}\right)\left(\frac{X}{0.1}\right)^{3/2}. \tag{6}$$

The amplitude of the quasi-periodic oscillation in the Fourier domain is determined by its duration and hence, depends strongly on the initial compactness of neutron stars and final product. Therefore, by observing the amplitude of this peak, we will be able to obtain information about the compactness of neutron stars before the merger, and final product. From gravitational waves emitted in the inspiraling phase with post Newtonian templates of waveforms [21], mass of two neutron stars, and hence, total mass will be determined [22]. This implies that we could constrain the maximum allowed mass of neutron stars, and hence, nuclear equations of state from the amplitude of the quasi-periodic oscillation emitted by the merged object.

Since the frequency of this Fourier peak is rather high, it will be difficult to detect by first generation, kilo-meter-size laser interferometers such as LIGO. However, the resonant-mass detectors and/or specially designed narrow band interferometers may be available in future, to detect such high frequency gravitational waves. These detectors will provide us a variety of information on neutron star physics.

V SUMMARY

We have performed fully GR simulations of merger of binary neutron stars. As demonstrated in this paper, the simulations are feasible stably and fairly accurately to yield scientific results.

One of the most interesting results found in this work is that the products after merger depend sensitively on the compactness of neutron stars before merger. If the total rest mass of the system is sufficiently (1.3–1.7 times depending on Γ) larger than the maximum rest mass of a spherical star in isolation, a black hole is formed, and otherwise, a massive neutron star is formed. It is noteworthy that the rest mass of the massive neutron star can be significantly larger than the maximum value for a spherical star of identical equation of state. The self-gravity of such high mass neutron stars can be supported by a rapid, differential rotation [11,10]. We also found that the difference of the final products is significantly reflected in the waveforms of gravitational waves, suggesting that detection of gravitational waves of high frequency could constrain the maximum allowed mass of neutron stars.

In the case of prompt black hole formation, the disk mass is found to be very small, i.e., less than 1% of the total rest mass. The main reason is that the specific angular momentum of all the fluid elements in binary neutron stars of irrotational velocity field just before the merger is too small and transport timescale of the angular momentum is not short enough to help the disk formation. It should be noted that this conclusion may hold only for binary neutron stars of equal (or nearly equal) mass. In binaries of a large mass ratio, the conclusion could be modified, because the neutron star of smaller mass may be tidally disrupted before the separation of two stars becomes small and hence, before the angular momentum of the system is not significantly dissipated by gravitational radiation. In this case, many of fluid elements in the neutron star of smaller mass may have a large angular momentum enough to form a disk during the merger. To clarify whether such scenario is promising or not, it is necessary to perform simulations for merger of binary neutron stars of unequal mass.

ACKNOWLEDGMENTS

We would like to thank J. C. Wheeler for inviting M.S. to this meeting to give an opportunity for presenting our works. We also thank T. Baumgarte, E. Gourgoulhon, T. Nakamura, K. Oohara and S. Shapiro for discussions. Numerical computations were performed on the FACOM VPP300/16R, VX/4R and VPP5000 machines in the data processing center of National Astronomical Observatory of Japan.

REFERENCES

1. For example, K. S. Thorne, in *Proceeding of Snowmass 95 Summer Study on Particle and Nuclear Astrophysics and Cosmology*, eds. E. W. Kolb and R. Peccei (World Scientific, Singapore, 1995), p. 398, and references therein.
2. E. S. Phinney, Astrophys. J. **380**, L17 (1991): R. Narayan, T. Piran and A. Shemi, Astrophys. J. **379**, L17 (1991).
3. T. Piran, this volume.
4. S. R. Kulkarni, this volume.
5. K. Oohara, T. Nakamura, and M. Shibata, Prog. Theor. Phys. Suppl. **128**, 183 (1997) for a review before 1997: For recent researches, e.g., J. A. Faber and F. A. Rasio, Phys. Rev. D **62**, 064012 (2000).
6. K. Oohara and T. Nakamura, Prog. Theor. Phys. Suppl. **136**, 270 (1999).
7. J. A. Font, M. Miller, W.-M. Suen, and M. Tobias, Phys. Rev. D **61**, 044011 (2000).
8. M. Shibata, Phys. Rev. D **60**, 104502 (1999).
9. M. Shibata, T. W. Baumgarte, and S. L. Shapiro, Phys. Rev. D **61**, 044012 (2000).
10. T. W. Baumgarte, S. L. Shapiro, and M. Shibata, Astrophys. J. Lett. **528**, L29 (2000).
11. M. Shibata and K. Uryū, Phys. Rev. D **61**, 064001 (2000).
12. M. Shibata, T. W. Baumgarte, and S. L. Shapiro, Astrophys. J. **542**, 453 (2000).
13. M. Shibata, Prog. Theor. Phys. **101**, 1199 (1999).
14. M. Shibata and T. Nakamura, Phys. Rev. D **52**, 5428 (1995).
15. B. J. van Leer, J. Comp. Phys. **23**, 276 (1977).

16. S. L. Shapiro and S. A. Teukolsky, *Black Holes, White Dwarfs, and Neutron Stars*, Wiley Interscience (New York, 1983).
17. C. S. Kochanek, Astrophys. J. **398**, 234 (1992): L. Bildsten and C. Cutler, *ibid*, **400**, 175 (1992).
18. M. Shibata, Phys. Rev. D **58**, 024012 (1998): S. A. Teukolsky, Astrophys. J. **504**, 442 (1998): See also, S. Bonazzola, E. Gourgoulhon and J.-A. Marck, Phys. Rev. D **56**, 7740 (1997): H. Asada, Phys. Rev. D **57**, 7292 (1998).
19. K. Uryū and Y. Eriguchi, Phys. Rev. D **61**, 124023 (2000): See also, E. Gourgoulhon et al., gr-qc/0007028 with regard to other approach.
20. K. Uryū, M. Shibata and Y. Eriguchi, Phys. Rev. D **62**, 104015 (2000).
21. L. Blanchet, B. R. Iyer, C. M. Will and A. G. Wiseman, Class. Quant. Grav. **13**, 575 (1996).
22. C. Cutler and E. E. Flanagan, Phys. Rev. D **49**, 2658 (1994).

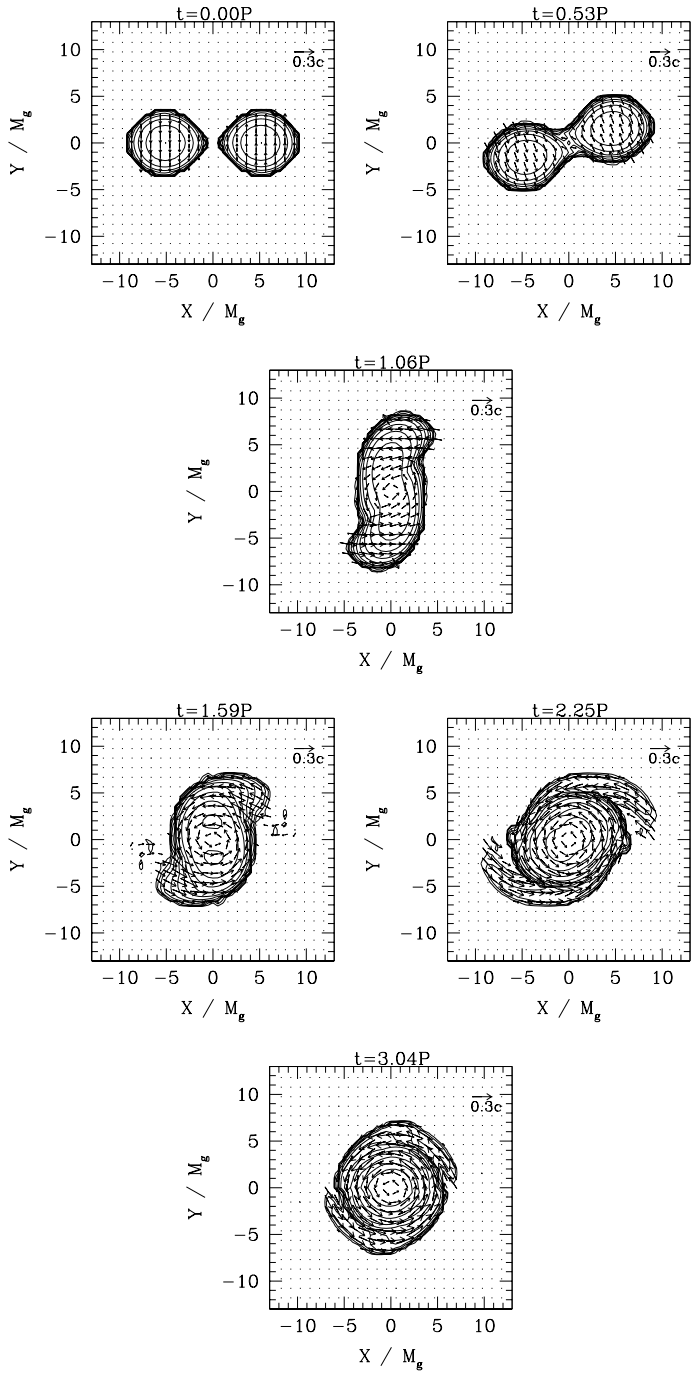

FIGURE 1. Snapshots of the density contours for ρ_* in the equatorial plane for model (A). The contour lines are drawn for $\rho_*/\rho_{*\ \max} = 10^{-0.3j}$, where $\rho_{*\ \max}$ denotes the maximum value of ρ_* at $t = 0$ (here $\bar{\rho}_{*\ \max} = 0.355$), for $j = 0, 1, 2, \cdots, 10$. The maximum density for ρ_* in the final panel is about 2.8 times larger than the initial value. Vectors indicate the local velocity field and the scale is as shown in the top left-hand frame. P denotes the orbital period of the initial quasiequilibrium ($P_{t=0}$). The length scale is shown in units of GM_g/c^2 where M_g is the gravitational mass at $t = 0$.

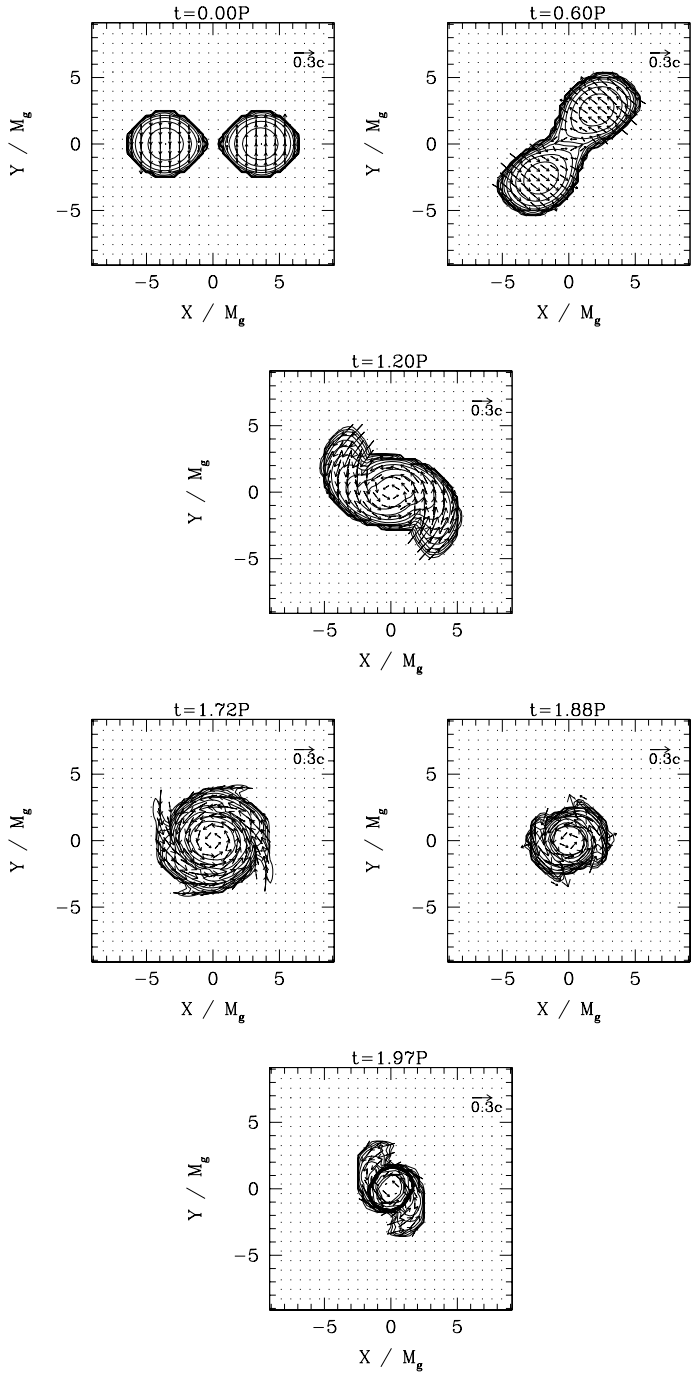

FIGURE 2. The same as 1, but for model (C). The contour lines are drawn for $\rho_*/\rho_{*\,\max} = 10^{-0.3j}$, where $\bar{\rho}_{*\,\max} = 0.757$, for $j = 0, 1, 2, \cdots, 10$. The maximum density for ρ_* in the final panel is about 80 times larger than the initial value. The thick solid circle in the final panel denotes the apparent horizon.

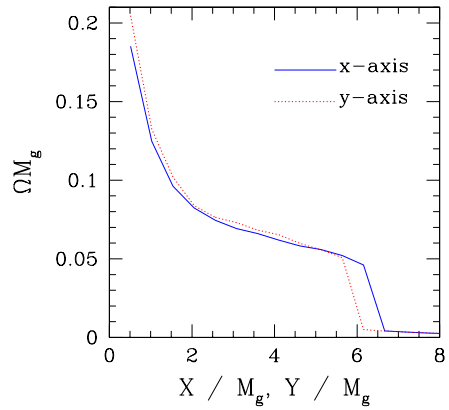

(a)

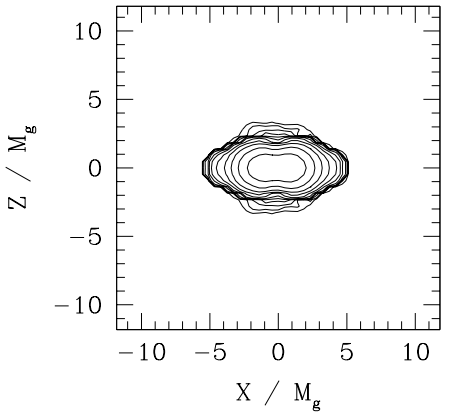

(b)

FIGURE 3. (a) The angular velocity in units of M_g^{-1} along x and y axes and (b) the density contour in x-z slices at $t = 3.04P_{t=0}$ for the merged object of model (A). The contour lines are drawn in the same manner as for Fig. 1.

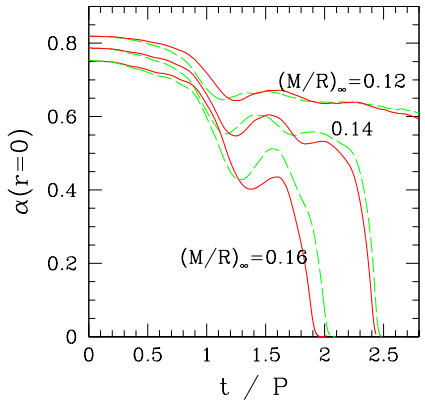

Fig. 4

Fig.

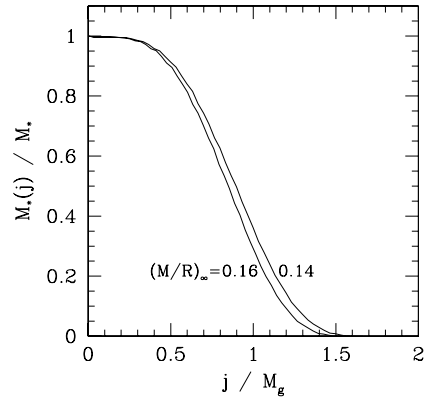

FIGURE 4. The lapse function α at $r = 0$ as a function of coordinate time for models (A)–(C). The solid and dashed lines denote the results for simulations with $(293, 293, 147)$ grid resolution and with $(193, 193, 97)$ grid resolution. For smaller scale simulations, the grid size is 116/96 times larger than that for larger scale simulations. (Namely, the outer boundaries along each axis are located $116L/146$ in these cases.)

FIGURE 5. $M_*(j)/M_*$ as a function of j/M_g for quasiequilibrium configurations (B) and (C).

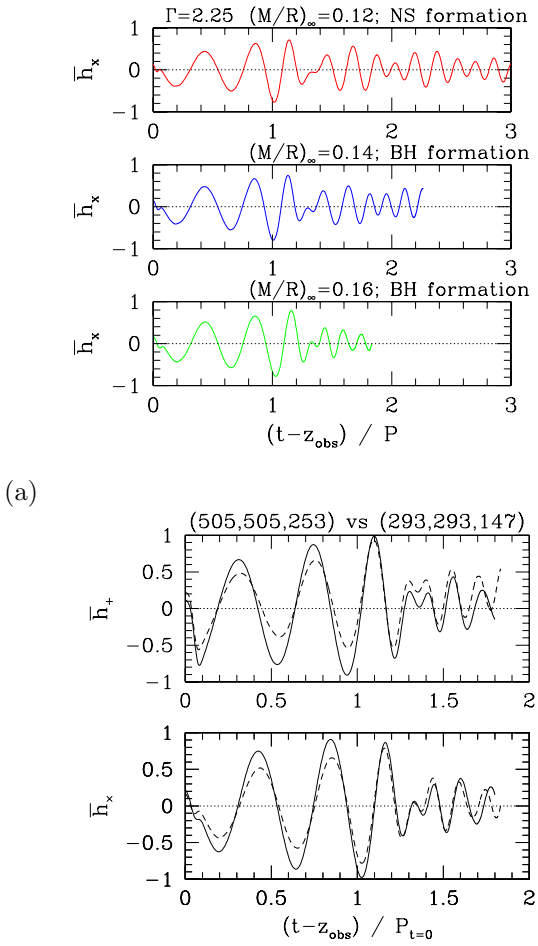

(a) (b)

FIGURE 6. (a) $\bar{h}_\times$ near the outer boundary along the z-axis as a function of retarded time (in units of P) for models (A)–(C) with $(293, 293, 147)$ grid size. P denotes $P_{t=0}$. (b) $\bar{h}_+$ and $\bar{h}_\times$ for model (C) with $(505, 505, 253)$ (solid line) and $(293, 293, 147)$ (dashed line) grid sizes.